Inorg. Chem. **2008**, *47*, 11745−11754

One- and Two-Electron Reduced 1,2-Diketone Ligands in $[Zn^{II}(L^{\bullet})_2(Et_2O)]$, $[Co^{II}(L^{\bullet})_2(Et_2O)]$, and $Na_2(Et_2O)_4[Co^{II}(L^{Red})_2]$

Geoffrey H. Spikes, Carsten Milsmann, Eckhard Bill, Thomas Weyhermüller, and Karl Wieghardt*

Max-Planck-Institut für Bioanorganische Chemie, Stiftstrasse 34-36, D-45470 Mülheim an der Ruhr, Germany

Received August 4, 2008

The reaction of 1,2-diketone bis(2,6-diisopropylphenyl)glyoxal (L^{Ox}) with $ZnCl_2$ or $CoCl_2$ (ratio 2:1) in dry diethyl ether with 2 equiv of sodium (per transition-metal ion) afforded the neutral complexes $[Zn^{II}(L^{\bullet})_2(Et_2O)]$ (**1**) and $[Co^{II}(L^{\bullet})_2(Et_2O)]$ (**2**), which were characterized by X-ray crystallography, magnetochemistry, IR, electron paramagnetic resonance, and UV−vis spectroscopy. When 4 equiv of sodium were added, complex $Na_2(Et_2O)_4[Co^{II}(L^{Red})_2]$ (**4**) was isolated, which included some crystals of a minor (<2%) product $Na(Et_2O)_2[Co^{III}(L^{Red})_2]$ (**3**). $(L^{\bullet})^-$ represents the π-radical monoanion of the 1,2-diketone, and $(L^{Red})^{2-}$ is its enediolate(2−) analogue. The electronic structures of **1**, **2**, and **4** have been elucidated by spectroscopy, and results are corroborated by broken-symmetry density functional theory calculations using the B3LYP functional. **1** possesses an $S = 0$ ground state with an excited triplet state that is 130 cm^{-1} higher in energy; **2** and **4** have an $S = {}^1/_2$ ground state. These complexes corroborate the notion that acyclic 1,2-diketones are redox noninnocent ligands.

1. Introduction

The coordination chemistry of acyclic 1,2-diketones and their one- and two-electron-reduced forms (Scheme 1) has not been investigated in the past in the same breadth as their benzene-type analogues, namely, catecholate(2−), *o*-benzosemiquinonate(1−), or their neutral *o*-benzoquinone form.[1] Only very recently have the first structurally characterized complexes containing the monoanionic π-radical anion, $(L^{\bullet})^-$ (Scheme 1), been reported from our laboratory: $[Ni^{I}(L^{\bullet})(cod)]^0$ (cod = cyclooctadiene), $[Fe^{III}(L^{\bullet})_3]^0$,[2] and $[Cr^{III}(L^{\bullet})_3]$.[3] Complexes containing 1,2-enediolate(2−) ligands have been reported,[4] and its two-electron-oxidized form, the neutral 1,2-diketone dibenzoyl (L^{Ox1}), has been crystallographically characterized in octahedral $[Ti^{IV}(L^{Ox1})Cl_4]$.[5]

We have also reported a mixed-valent iron species $[Na(DME)_3][Fe^{II}Fe^{III}Br_2(L^{Red})_2(DME)]$,[6] where DME represents dimethoxyether and $(L^{Red})^{2-}$ is the doubly reduced enediolate(2−) of bis(2,6-diisopropylphenyl)glyoxal as in $Na_2(Et_2O)_2[V^{IV}(L^{Red})_3]$.[3] Thus, the acyclic 1,2-diketone ligand has been structurally characterized in three different oxidation levels, namely, the neutral 1,2-diketone, its one-electron-reduced π-radical monoanion, and its doubly reduced 1,2-enediolate(2−) form (Scheme 1).

The most salient observation pertains to the fact that the C−O bond length is a characteristic marker for the respective oxidation level of the ligand: (a) in the O,O′-coordinated, neutral diketone form, the C═O distances are short at ∼1.25 Å (double bond), (b) in the corresponding π-radical monoanions, these bonds are longer at ∼1.29 Å, and (c) in the 1,2-enediolate(2−) form, they are at ∼1.35 Å (single bond). In contrast, the C−C bond of the dicarbonyl group decreases in the same series from 1.56 Å (single bond) in the 1,2-diketones to ∼1.46 Å in the radical monoanion to ∼1.39 Å in 1,2-enediolate(2−).

* To whom correspondence should be addressed. E-mail: wieghardt@mpi-muelheim.mpg.de.

(1) Pierpont, C. G.; Lange, C. W. *Prog. Inorg. Chem.* **1994**, *41*, 331.
(2) Spikes, G. H.; Bill, E.; Weyhermüller, T.; Wieghardt, K. *Angew. Chem., Int. Ed.* **2008**, *47*, 2973.
(3) Spikes, G. H.; Sproules, S.; Bill, E.; Weyhermüller, T.; Wieghardt, K. *Inorg. Chem.* **2008**, submitted for publication.
(4) (a) Hofmann, P.; Frede, M.; Stauffert, P.; Lasser, W.; Thewalt, U. *Angew. Chem., Int. Ed.* **1985**, *24*, 712. (b) Erker, G.; Czisch, P.; Schlund, R.; Angermund, K.; Krüger, C. *Angew. Chem., Int. Ed. Engl.* **1986**, *25*, 364. (c) Song, L.-C.; Liu, P.-C.; Han, C.; Hu, Q. M. *J. Organomet. Chem.* **2002**, *648*, 119. (d) Chisholm, M. H.; Huffman, J. C.; Ratermann, A. L. *Inorg. Chem.* **1983**, *22*, 4100. (e) Sugawara, K.-I.; Hikichi, S.; Akita, M. *J. Chem. Soc., Dalton Trans.* **2002**, 4514. (f) Weinert, C. S.; Fenwick, P. E.; Rothwell, I. P. *Dalton Trans.* **2003**, 532. (g) Asadi, A.; Eaborn, C.; Hill, M. S.; Hitchcock, P. B.; Meehan, M. M.; Smith, J. D. *Organometallics* **2002**, *21*, 2430.
(5) Carofiglio, T.; Cozzi, P. G.; Floriani, C. *Organometallics* **1993**, *12*, 2726.
(6) Spikes, G. H.; Bill, E.; Weyhermüller, T.; Wieghardt, K. *Chem. Commun.* **2007**, 4339.

10.1021/ic801470p CCC: $40.75 © 2008 American Chemical Society
Published on Web 11/12/2008

Scheme 1. Observed Redox States and Bond Lengths for the Bulky 1,2-Diketone Bis(2,6-diisopropylphenyl)glyoxal and Complexes

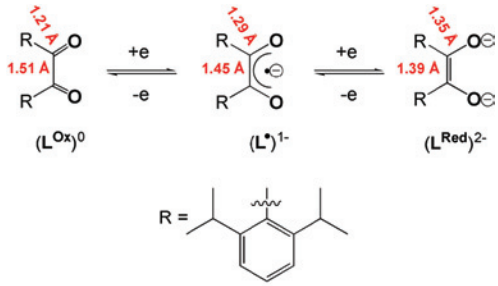

Complexes

$[Zn^{II}(L^{\bullet})_2(Et_2O)]$	S = 0, 1	1
$[Co^{II}(L^{\bullet})_2(Et_2O)]$	S = 1/2	2
$Na(Et_2O)_2[Co^{III}(L^{Red})_2] \cdot Et_2O$		3
$Na_2(Et_2O)_4[Co^{II}(L^{Red})_2]$	S = 1/2	4

Chart 1

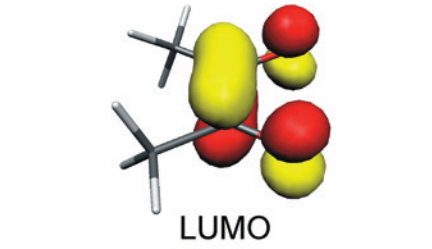

	$(L^{OX})^0$	$(L^{\bullet})^{1-}$	$(L^{Red})^{2-}$
C-O, Å	1.25	1.29	1.35
C-C, Å	1.56	1.46	1.39
C-N, Å	1.29	1.35	1.40
C-C, Å	1.47	1.40	1.36
C-S, Å	-----	1.74	1.76
C-C, Å	-----	1.365	1.34

Chart 1 displays the lowest unoccupied molecular orbital (LUMO) of the *cis*-1,2-diketone, which is antibonding with respect to the two C−O bonds but bonding to the C−C bond. Thus, successive one- and two-electron reduction (filling the LUMO) leads to a lengthening of the C−O bonds but a shortening of the C−C bond.

Interestingly, the same trends have been observed for a large number of N,N′-disubstituted α-diimines (which also exist in three oxidation levels) and their coordination compounds.[7,8] Furthermore, dithiolenes have been discussed in similar terms.[9] Also, the *o*-iminoketones have been shown to exist in three different oxidation levels.[10]

In this Article, we report the syntheses and characterization of three new complexes shown in Scheme 1, which contain either two π-radical anions as in **1** and **2** or two fully reduced 1,2-enediolate(2−) ligands as in **4** (and possibly **3**). We analyze their electronic structure by electron paramagnetic resonance (EPR) spectroscopy and magnetochemistry and corroborate the results by density functional theory (DFT) calculations at the B3LYP level.

2. Experimental Section

All manipulations were carried out in a glovebox with an argon atmosphere containing less than 1 ppm of O_2 and less than 1 ppm of H_2O. Carefully dried and deoxygenated solvents were used. The ligand bis(2,6-diisopropylphenyl)glyoxal was prepared as described in ref 6.

$[Zn^{II}(L^{\bullet})_2(Et_2O)]$ (1). To a solution of bis(2,6-diisopropylphenyl)glyoxal (L; 0.40 g, 1.06 mmol) in dry diethyl ether (10 mL) was added $ZnCl_2$ (72 mg, 0.53 mmol) and sodium (24.0 mg, 1.06 mmol) with stirring at 20 °C. The pale-yellow solution turned green/yellow over 48 h. Removal of the solvent in vacuo resulted in a dark residue, which was extracted in Et_2O (3 mL) and filtered. Slow evaporation of the solvent yielded dark crystals of **1** in a moderate yield (220 mg, 46%). UV−vis [Et_2O; λ, nm (ε, M^{-1} cm^{-1})]: 600, sh (620), 360 (1.25×10^4). IR (KBr disk): 1592 (s), 1572 (w), 1472 (s), 1452 (s), 1396 (s, ν(C−O)), 1055 (s), 1027 (m), 927 (s), 804 (s), 763 (s), 719 (m) cm^{-1}. Anal. Calcd for $C_{56}H_{78}O_5Zn$: C, 75.0; H, 8.77. Found: C, 74.8; H, 8.71.

$[Co^{II}(L^{\bullet})_2(Et_2O)]$ (2). Compound **2** was prepared as described above for **1** by using anhydrous $CoCl_2$ (68 mg, 0.53 mmol) instead of $ZnCl_2$. Dark crystals suitable for X-ray crystallography were obtained in good yield (296 mg, 63%). UV−vis [Et_2O; λ, nm (ε, M^{-1} cm^{-1})]: 600, sh (1.2×10^3), 360 (1.2×10^4). IR (KBr disk): 1592 (s), 1573 (w), 1461 (s), 1441 (s), 1397 (s, ν(C−O)), 1381 (s), 1354 (s), 1308 (m), 1242 (m), 1219 (m), 1190 (s), 1098 (m), 1061 (s), 1031 (m), 927 (s), 804 (s), 763 (s), 719 (m) cm^{-1}. Anal. Calcd for $C_{56}H_{78}O_5Co$: C, 75.6; H, 8.83. Found: C, 75.7; H, 8.73.

$Na(Et_2O)_2[Co^{III}(L^{Red})_2] \cdot Et_2O$ (3). We have as yet not been able to prepare this complex in a pure form in a reproducible fashion. We picked a single crystal from a crude sample of **2** (see above) for X-ray crystallography.

$Na_2(Et_2O)_4[Co^{II}(L^{Red})_2]$ (4). To a solution of bis(2,6-diisopropylphenyl)glyoxal (400 mg, 1.06 mmol) in diethyl ether (10 mL) was added with stirring at ambient temperature $CoCl_2$ (68 mg, 0.53 mmol) and sodium (46.0 mg, 2.12 mmol). The pale-yellow solution turned deep red over 48 h. Removal of the solvent in vacuo resulted in a dark residue, which was extracted in Et_2O (3 mL) and filtered. Slow evaporation of the solvent yielded dark-red crystals of **4** in moderate yield (180 mg, 29%). Inspection of the crude crystalline sample under a microscope showed (at times) the presence of a few differently shaped crystals, one of which was characterized by X-ray crystallography as **3**. UV−vis [Et_2O; λ, nm (ε, M^{-1} cm^{-1})]: 540, sh (1.25×10^3), 460 (2.8×10^3), 360 (1.0×10^4). IR (KBr, disk): 1589 (s, ν(C═C)), 1573 (m), 1556 (m), 1463 (s), 1459 (s),

(7) van Koten, G.; Vrieze, K. *Adv. Organomet. Chem.* **1982**, *21*, 151.

(8) (a) Gardiner, M. G.; Hanson, G. R.; Henderson, M. J.; Lee, F. C.; Raston, C. L. *Inorg. Chem.* **1994**, *33*, 2456. (b) Rijnberg, E.; Richter, B.; Thiele, K.-H.; Boersma, J.; Veldman, N.; Spek, A. L.; van Koten, G. *Inorg. Chem.* **1998**, *37*, 56. (c) Khusniyarov, M. M.; Harms, K.; Burghaus, O.; Sundermeyer, J. *Eur. J. Inorg. Chem.* **2006**, *15*, 2985. (d) Muresan, N.; Chlopek, K.; Weyhermüller, T.; Neese, F.; Wieghardt, K. *Inorg. Chem.* **2007**, *46*, 5327. (e) Muresan, N.; Weyhermüller, T.; Wieghardt, K. *Dalton Trans.* **2007**, 4390. (f) Muresan, N.; Lu, C. C.; Ghosh, M.; Peters, J. C.; Abe, M.; Henling, L. M.; Weyhermüller, T.; Bill, E.; Wieghardt, K. *Inorg. Chem.* **2008**, *47*, 4579. (g) Kreisel, K. A.; Yap, G. P. A.; Theopold, K. M. *Inorg. Chem.* **2008**, *47*, 5293. (h) Ghosh, M.; Sproules, S.; Weyhermüller, T.; Wieghardt, K. *Inorg. Chem.* **2008**, *47*,in press.

(9) (a) Kirk, M. L.; McNaughton, R. L.; Helton, M. E. *Prog. Inorg. Chem.* **2004**, *52*, 111. (b) Ray, K.; Petrenko, T.; Wieghardt, K.; Neese, F. *Dalton Trans.* **2007**, 1552. (c) Lim, B. S.; Fomitchev, D. V.; Holm, R. H. *Inorg. Chem.* **2001**, *40*, 4257.

(10) Lu, C. C.; Bill, E.; Weyhermüller, T.; Bothe, E.; Wieghardt, K. *Inorg. Chem.* **2007**, *46*, 7880.

Table 1. Crystallographic Data for **1**−**4**

	1	**2**	**3**	**4**
chemical formula	$C_{56}H_{78}O_5Zn$	$C_{56}H_{78}CoO_5$	$C_{64}H_{98}CoNaO_7$	$C_{68}H_{108}CoNa_2O_8$
fw	896.55	890.11	1061.34	1158.45
space group	$P2_1/c$ (No. 14)	$P2_1/c$ (No. 14)	$P\bar{1}$ (No. 2)	$P\bar{1}$ (No. 2)
a, Å	17.037(2)	17.1093(7)	10.2350(8)	10.9830(7)
b, Å	14.7796(13)	14.8368(7)	12.7244(13)	13.5130(9)
c, Å	20.370(2)	20.4430(11)	13.1900(13)	14.0769(9)
α, deg	90	90	71.472(4)	66.691(3)
β, deg	98.350(2)	98.350(2)	74.950(5)	69.881(3)
γ, deg	90	90	88.420(5)	67.117(3)
V, Å	5074.8(9)	5135.9(4)	1570.1(3)	1722.5(2)
Z	4	4	1	1
T, K	100(2)	100(2)	100(2)	100(2)
ρ_{calcd}, g cm^{-3}	1.173	1.151	1.123	1.117
reflns collcd/$2\Theta_{max}$	206 811/65.00	150 933/66.82	17 980/55.00	47 417/60.00
unique reflns/$I > 2\sigma(I)$	18 352/15 271	19 494/15 331	7078/5084	10 035/8369
no. of param/restraints	591/8	591/8	420/56	370/0
λ, Å/μ(Kα), cm^{-1}	0.710 73/5.29	0.710 73/3.79	0.710 73/3.28	0.710 73/3.11
R1 [a]/GOF [b]	0.0339/1.077	0.0379/1.015	0.0607/1.029	0.0394/1.028
wR2 [c] [$I > 2\sigma(I)$]	0.0897	0.0919	0.1373	0.0961
residual density, e Å^{-3}	+0.84/−0.51	+0.50/−0.39	+0.45/−0.45	+1.06/−0.31

[a] Observation criterion: $I > 2\sigma(I)$. R1 = $\sum||F_o| - |F_c||/\sum|F_o|$. [b] GOF = $[\sum[w(F_o^2 - F_c^2)^2]/(n-p)]^{1/2}$. [c] wR2 = $[\sum[w(F_o^2 - F_c^2)^2]/\sum[w(F_o^2)^2]]^{1/2}$ where $w = 1/\sigma^2(F_o^2) + (aP)^2 + bP$, $P = (F_o^2 + 2F_c^2)/3$.

1381 (s), 1350 (m), 1267 (m), 1239 (m), 1219 (m), 1129 (s), 1096 (s, ν(CO)), 1048 (s), 1024 (s), 940 (s), 844 (w), 804 (w), 760 (s), 727 (w) cm^{-1}. Anal. Calcd for $C_{68}H_{108}O_8CoNa_2$: C, 70.50; H, 9.40. Found: C, 70.25; H, 9.26.

Physical Measurements. Electronic spectra of complexes were recorded with a Perkin-Elmer double-beam photometer (300−2000 nm). Cyclic voltammograms were recorded with an EG&G potentiostat/galvanostat. Variable-field (0.01 or 1 T), variable-temperature (4−300 K) magnetization data were recorded on a SQUID magnetometer (MPMS Quantum Design). The experimental magnetic susceptibility data were corrected for underlying diamagnetism using tabulated Pascal's constants. X-band EPR spectra were recorded on a Bruker ESP 300 spectrometer.

Calculations. All calculations were done with the *ORCA* program package.[11] The geometry optimizations were carried out at either the B3LYP[12] or BP86[13] levels of DFT. The all-electron Gaussian basis sets used were those reported by the Ahlrichs group.[14,15] For zinc, cobalt, sodium, and oxygen atoms, the triple-ζ-quality basis sets with one set of polarization functions were used (TZVP).[14] The carbon and hydrogen atoms were described by smaller polarized split-valence SV(P) basis sets (double-ζ quality in the valence region with a polarizing set of d functions on the non-hydrogen atoms).[15] The auxiliary basis sets for all atoms used to expand the electron density in the calculations were chosen to match the orbital basis. The self-consistent-field calculations were tightly converged ($1 \times 10^{-8} E_h$ in energy, $1 \times 10^{-7} E_h$ in the density change, and 1×10^{-7} in the maximum element of the DIIS[16] error vector). The energy search for all complexes was carried out in redundant internal coordinates without imposing geometry constraints. The geometries were considered converged after the energy change was less than $5 \times 10^{-6} E_h$, the gradient norm and maximum gradient element were smaller than 1×10^{-4} and $3 \times 10^{-4} E_h$/bohr, respectively, and the root-mean-square and maximum displacements of the atoms were smaller than 2×10^{-3} and 4×10^{-3} bohr, respectively. Corresponding[17] and quasi-restricted[18] orbitals and density plots were obtained by the program *Molekel*.[19] We describe our computational results for **1** and **2** containing noninnocent ligands by using the broken-symmetry (BS) approach.[20−22]

X-ray Crystallographic Data Collection and Refinement of the Structures. A dark-red single crystal of **2** and red-orange crystals of **1**, **3**, and **4** were coated with perfluoropolyether, picked up with nylon loops, and mounted in the cold nitrogen stream of the diffractometer. A Bruker-Nonius Kappa CCD diffractometer equipped with a molydenum-target rotating-anode X-ray source and a graphite monochromator (Mo Kα, $\lambda = 0.710\,73$ Å) was used throughout. Final cell constants were obtained from least-squares fits of all measured reflections. Intensity data of **1**, **2**, and **4** were corrected for absorption using intensities of redundant reflections. The Gaussian absorption correction routine embedded in XPREP[23] was used to correct intensity data of compound **3**. The structures were readily solved by Patterson methods and subsequent difference Fourier techniques. The Bruker *ShelXTL*[23] software package was used for solution, refinement, and artwork of the structures. All non-hydrogen atoms were anisotropically refined, and hydrogen atoms were placed at calculated positions and refined as riding atoms with isotropic displacement parameters. Crystallographic data of the compounds are listed in Table 1.

The coordinated diethyl ether molecules in complexes **1** and **2** were found to be disordered over two sites. Split atom models with restrained atomic displacement parameters (EADP) and restrained bond lengths (SAME and SADI) yielded occupation ratios of about 0.7:0.3 in the case of **1** and 0.86:0.14 for **2**.

(11) Neese, F. *ORCA, an Ab Initio Density Functional and Semiempirical Electronic Structure Program Package*, version 2.6, revision 35; Max Planck Institute for Bioinorganic Chemistry: Mülheim, Germany, 2008.
(12) (a) Becke, A. D. *J. Chem. Phys.* **1993**, *98*, 5648. (b) Lee, C. T.; Yang, W. T.; Parr, R. G. *Phys. Rev. B* **1988**, *37*, 785.
(13) (a) Becke, A. D. *J. Chem. Phys.* **1986**, *84*, 4524. (b) Perdew, J. P. *Phys. Rev. B* **1986**, *33*, 8822.
(14) Schäfer, A.; Horn, H.; Ahlrichs, R. *J. Chem. Phys.* **1992**, *97*, 2751.
(15) Schäfer, A.; Huber, C.; Ahlrichs, R. *J. Chem. Phys.* **1994**, *100*, 5829.
(16) (a) Pulay, P. *Phys. Chem. Lett.* **1980**, *73*, 393. (b) Pulay, P. *J. Comput. Chem.* **1992**, *3*, 556.
(17) Neese, F. *J. Phys. Chem. Solids* **2004**, *65*, 781.
(18) Schöneboon, J. C.; Neese, F.; Thiele, W. *J. Am. Chem. Soc.* **2005**, *127*, 5840.
(19) Molekel, Advanced Interactive 3D-Graphics for Molecular Sciences, available at http://www.cscs.ch/molekel.
(20) Noodleman, L.; Peng, C. Y.; Case, D. A.; Monesca, J. M. *Coord. Chem. Rev.* **1995**, *144*, 199.
(21) (a) Noodleman, L. *J. Chem. Phys.* **1981**, *74*, 5737. (b) Noodleman, L.; Case, D. A.; Aizman, A. *J. Am. Chem. Soc.* **1988**, *110*, 1001. (c) Noodleman, L.; Davidson, E. R. *Chem. Phys.* **1986**, *109*, 131. (d) Noodleman, L.; Norman, J. G.; Osborne, J. H.; Aizman, A.; Case, D. A. *J. Am. Chem. Soc.* **1985**, *107*, 3418.
(22) Kapre, R. R.; Bothe, E.; Weyhermüller, T.; DeBeer George, S.; Muresan, N.; Wieghardt, K. *Inorg. Chem.* **2007**, *46*, 7827.
(23) *ShelXTL 6.14*; Bruker AXS Inc.: Madison, WI, 2003.

Table 2. Selected Bond Distances (Å)

	1	2	3	4
M−O63	2.0825(13)	2.0643(9)		
M−O1	1.9705(7)	1.9445(7)	1.837(2)	1.8659(8)
M−O2	2.0511(8)	2.0711(7)	1.831(2)	1.8767(9)
M−O31	1.9712(7)	1.9367(7)		
M−O32	2.0542(8)	2.0950(7)		
O1−C1	1.290(1)	1.299(1)	1.345(3)	1.373(1)
O2−C2	1.281(1)	1.284(1)	1.345(3)	1.374(1)
C1−C2	1.440(1)	1.445(1)	1.384(3)	1.360(2)
O31−C31	1.288(1)	1.297(1)		
O32−C32	1.281(1)	1.281(1)		
C31−C32	1.439(1)	1.443(1)		
Na−O2			2.296(3)	2.254(1)
Na−O40			2.311(2)	2.328(1)
Na−O50			2.298(4)	2.344(1)
Na−O1				2.246(1)

The crystal structure of **3** appeared to be severely disordered on a crystallographic center of inversion. Because of this inversion center, two sodium ion positions are generated, which are each only half-occupied. The sodium ion coordinates to two ligand oxygen atoms, namely, O(1) and O(82A), and furthermore to the oxygen atoms of two diethyl ether molecules, which for the above-mentioned reason are also only half-occupied. In the crystal lattice, coordination of an $Na(OEt_2)_2$ entity on one side of the complex molecule leaves a void on the other side, which is filled with a third molecule of ether. This solvent molecule again has an occupation factor of only 0.5. To rule out that the structure is, in fact, noncentrosymmetric, it was also carefully refined in space group $P1$ but the disorder of the sodium ion and ether molecules persisted, which is a strong indication that the space group $P\bar{1}$ is appropriate in this case. To address the complicated disorder of this structure, a total of 56 restraints (EADP, SADI, and SAME) were used to improve the geometries of the diethyl ether molecules.

3. Results and Discussion

3.1. Syntheses. The reaction of 2 equiv of the neutral ligand bis(2,6-diisopropylphenyl)glyoxal, $(L^{Ox})^0$, with 1 equiv of anhydrous $Zn^{II}Cl_2$ or $Co^{II}Cl_2$ in diethyl ether and 2 equiv of sodium metal at room temperature under strictly anaerobic conditions affords in moderate to good yields the crystalline samples of the neutral, five-coordinate complexes $[M(L^{\bullet})_2(Et_2O)]$ [M = Zn (**1**), Co (**2**)] where $(L^{\bullet})^-$ represents the one-electron-reduced monoanionic π radical of the neutral 1,2-diketone L^{Ox}. Both species are dark red.

When the ratio $CoCl_2/L^{Ox}/Na$ was changed to 1:2:4 using otherwise identical reaction conditions, the fully reduced form of **2**, namely **4**, was isolated as dark-red crystals. $(L^{Red})^{2-}$ is the enediolate(2−) form of the neutral ligand. Interestingly, in some cases the microcrystalline material obtained in the above fashion contained a few crystals of a different habitus than the bulk material. One of the crystals was suitable for single-crystal crystallography. As it turns out, this crystal consists of **3**, which is the one-electron oxidized form of **4**. This oxidation may be triggered by traces of adventitiously present dioxygen. We have as yet not been able to synthesize **3** in pure form.

3.2. Crystal Structures. The crystal structures of **1**−**4** have been determined at 100(2) K by using Mo Kα radiation ($\lambda = 0.71073$ Å). Crystallographic details are given in Table 1; Table 2 summarizes important bond distances. Figure 1 displays the structures of neutral $[Zn(L^{\bullet})_2(Et_2O)]$ in crystals of **1** and the corresponding molecule $[Co^{II}(L^{\bullet})_2(Et_2O)]$ in crystals of **2**, whereas Figure 2 shows the structure of the ion pair $Na(Et_2O)_2[Co(L^{Red})_2]$ in crystals of **3** and the structure of **4**.

The neutral molecule in **1** consists of two O,O′-coordinated 1,2-diketonate(1−) π-radical anions and an O-coordinated diethyl ether ligand in an apical position of the square-base-pyramidal ZnO_5 polyhedron. Significantly, the relatively long average C−O bond at 1.285 ± 0.003 Å and the relatively short avearge C−C distance at 1.440 ± 0.003 Å of the 1,2-dicarbonyl units are indicative of the presence of two π-radical monoanions $(L^{\bullet})^-$ (Scheme 1).

It is worth mentioning that the metrical details of the two five-membered chelate rings are within experimental error identical (both rings are not related by crystallographically imposed symmetry). This finding rules out an unsymmetrical charge distribution as in hypothetical $[Zn^{II}(L^{Red})^{2-}(L^{Ox})^0(Et_2O)^0]$. In conjunction with the magnetic susceptibility measurements and the EPR spectrum (see below), **1** may serve as a benchmark for coordination compounds with O,O′-coordinated 1,2-diketonate(1−) π-radical ligands.

The structure of the neutral molecule $[Co^{II}(L^{\bullet})_2(Et_2O)]$ in crystals of **2** is very similar to that of the zinc complex **1**. Again the average C−O distance at 1.290 ± 0.003 Å and the average C−C bond of the 1,2-dicarbonyl units at 1.444 ± 0.003 Å are only compatible with the 1,2-diketonate(1−) π-radical oxidation level, which renders the central metal ion Co^{II} d^7. The geometrical details of both (crystallographically independent) five-membered chelate rings are within experimental error (3σ) identical, ruling out a structure as in $[Co^{II}(L^{Red})^{2-}(L^{Ox})^0(Et_2O)]^0$. An O-coordinated diethyl ether ligand renders the cobalt ion five-coordinate (square-base-pyramidal).

The structure of the neutral molecule $Na_2(Et_2O)_4[Co^{II}(L^{Red})_2]^0$ in crystals of **4** is quite remarkable. In contrast to **2**, the central cobalt(II) ion in **4** is only four-coordinate. The two five-membered chelate rings form a dihedral angle of 0°; the CoO_4 unit possesses a crystallographically imposed square-planar geometry.

Interestingly, the four carbonyl oxygen donor atoms form Na−O bonds to two sodium cations, which, in turn, are each oxygen-bound to two terminal diethyl ether ligands. The NaO_4 polyhedron is distorted tetrahedral. Thus, the square-planar complex $[Co^{II}(L^{Red})_2]^{2-}$ is a dianion.

The metrical details of the two identical five-membered chelate rings indicate the presence of two O,O′-coordinated 1,2-enediolate(2−) ligands with two long C−O bonds at 1.373 ± 0.001 Å characteristic of a C−O single bond and a short C−C bond of the dicarbonyl unit at 1.360 ± 0.006 Å indicative of a C=C double bond (Scheme 1). The ligands $(L^{Red})^{2-}$ are diamagnetic, closed-shell dianions, and the central cobalt ion possesses a +II oxidation state (d^7) with an $S_{Co} = {}^1/_2$ ground state.[26]

The structure of the ion pair $Na(Et_2O)_2[Co(L^{Red})_2]$ in **3** is very similar to that of the corresponding entity in **4**, but it contains only one $[Na(Et_2O)_2]^+$ unit per cobalt ion, which would correspond to a one-electron oxidation of **4** with concomitant loss of a sodium cation (and two diethyl ether ligands). The

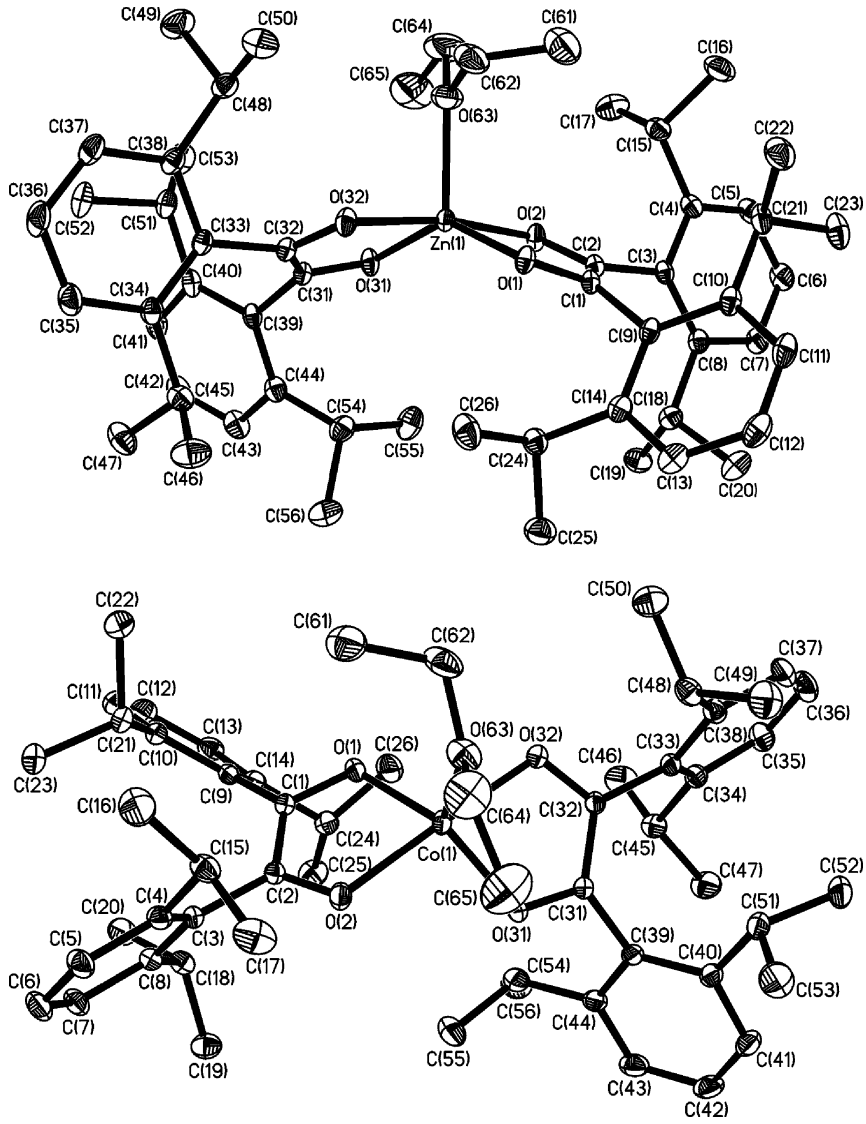

Figure 1. Perspective view of the neutral molecule $[Zn^{II}(L^{\bullet})_2(Et_2O)]$ in crystals of **1** (top) and the corresponding neutral molecule in crystals of **2** at the 50% probability level (bottom).

question arising concerns the locus of this one-electron oxidation: is it ligand-based, yielding a $[Co^{II}(L^{\bullet})(L^{Red})]^-$ monoanion, or is it metal-based, affording a central cobalt(III) ion as in $[Co^{III}(L^{Red})_2]^-$? The two five-membered chelate rings of the square-planar $Co(L)_2$ entity in **3** are crystallographically identical, and the geometrical details of the ligands are very similar to those in **4**. Thus, we propose that **3** contains a central cobalt(III) ion and two fully reduced 1,2-enediolate(2−) ligands. This is corroborated by the fact that the average Co−O bond length in **3** at 1.834 ± 0.006 Å is significantly shorter than the corresponding bonds in **4** at an average of 1.871 ± 0.003 Å ($\Delta = -0.037$ Å), which we would ascribe to a metal-centered reduction: $Co^{III} \rightarrow Co^{II}$ on going from **3** to **4**.

3.3. Vibrational Spectroscopy. If the variation of the C−O and (O)C−C(O) bond lengths as a function of the oxidation level, i.e., 1,2-diketone, 1,2-diketonate(1−) π-radical anion or 1,2-enediolate(2−), is as depicted in Scheme 1, one would expect the ν(C−O) stretching frequency of such a ligand in a given coordination complex to be a sensitive marker for the given oxidation level. This has been reported to be the case for complexes containing O,O′-coordinated catecholate(2−), *o*-benzosemiquinate(1−) π-radicals, or neutral *o*-benzosemiquinone ligands.[1] Table 3 summarizes the observed ν(CO) stretching frequencies of the free ligand L^{Ox}, an octahedral titanium(IV) complex containing an O,O′-coordinated dibenzoyl ligand $[Ti^{IV}(L^{Ox1})Cl_4]^0$, the present complexes **1**, **2**, and **4**, and the previously reported complexes $[Fe^{III}(L^{\bullet})_3]^0$ and $Na_2(Et_2O)_2[V^{IV}(L^{Red})_3]$.

From this data, it is clearly established that O,O′-coordinated 1,2-diketones exhibit a ν(C=O) stretching frequency in the range 1600−1700 cm^{-1}, whereas the corresponding π-radical monoanions display this mode in the range 1390−1450 cm^{-1}, and in the fully reduced 1,2-enediolate(2−) complexes, the ν(C−O) stretch is shifted to even lower energy (1050−1150 cm^{-1}).

3.4. Magnetochemistry and EPR Spectroscopy. From temperature-dependent magnetic susceptibility measurements (2−300 K, 1.0 T), the temperature dependence of the effective magnetic moment, μ_{eff}/μ_B, of **1** has been established and is shown in Figure 3. The values of μ_{eff} decrease monotonically from 2.2 μ_B at 290 K to 0.38 μ_B at 2 K. This

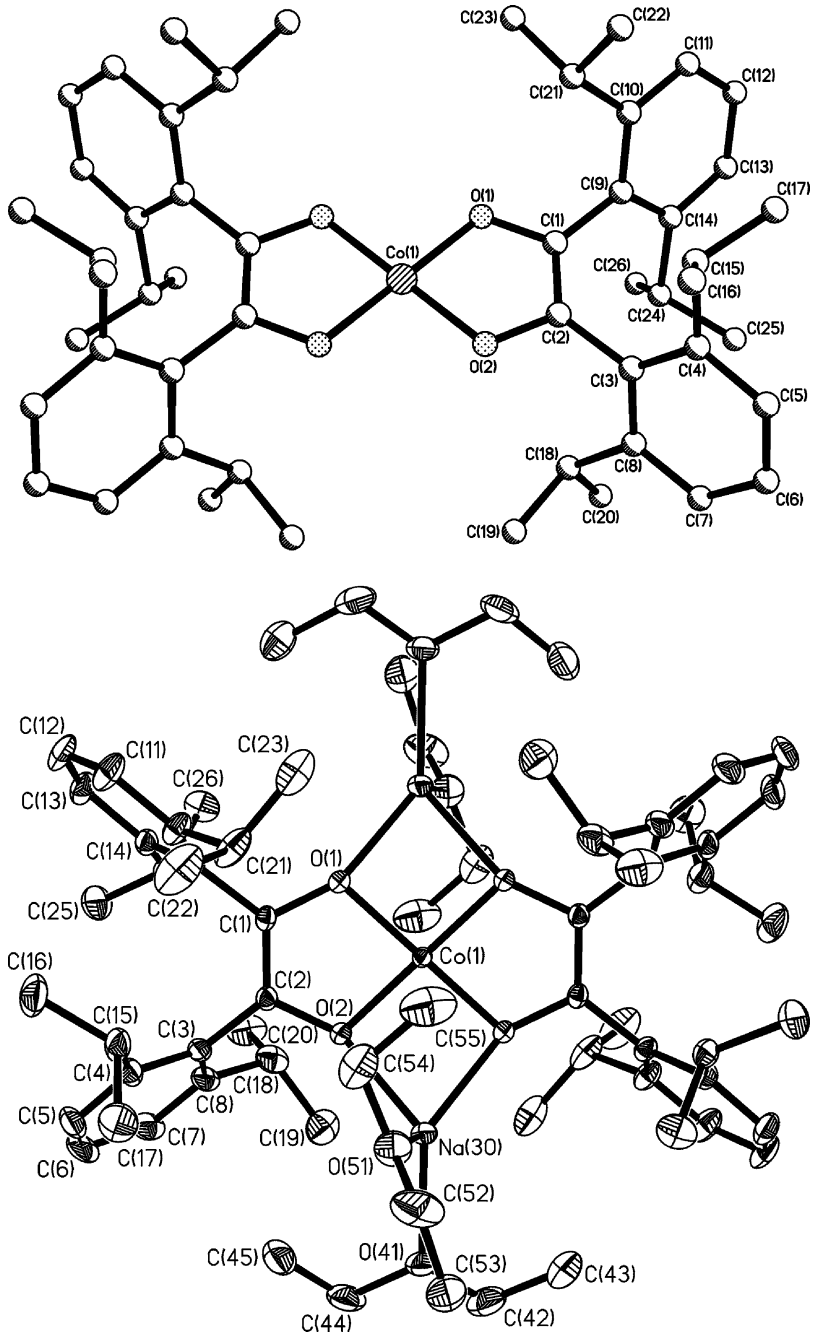

Figure 2. Perspective view of the monoanion $[Co^{III}(L^{Red})_2]^-$ in crystals of **3** (top; the sodium ion and diethyl ether molecules are not shown for the sake of clarity) and of $Na_2(Et_2O)_4[Co^{II}(L^{Red})_2]$ in **4** (bottom, 50% probability level).

Table 3. ν(C−O) Stretching Frequencies

		ν (C−O), cm^{-1}
free ligand L^{Ox}[a]		1700
$[Ti^{IV}(L^{Ox1})Cl_4]$ [b]		1662
$[Zn^{II}(L^{\bullet})_2]$	**1**	1396
$[Fe^{III}(L^{\bullet})_3]$[c]		1410
$[Co^{II}(L^{\bullet})_2(Et_2O)]$	**2**	1397
$[Co^{II}(L^{Red})_2]Na_2(Et_2O)_4$	**4**	1098
$[V^{IV}(L^{Red})_3]^{2-}Na_2(Et_2O)_2$[d]		1100

[a] Reference 6. [b] $(L^{Ox1})^0$ represents the ligand dibenzoyl.[5] [c] Reference 2. [d] Reference 3.

behavior has been successfully modeled assuming the presence of two π-radical anions, $(L^{\bullet})^-$, per diamagnetic zinc(II) ion, where the spins couple intramolecularly in an antiferromagnetic fashion. By using the usual exchange Hamiltonian $H_{ex} = -2JS_{rad1}\cdot S_{rad2}$ with $S_{rad1} = S_{rad2} = {}^1/_2$ and a g value of 2.006 taken from EPR spectroscopy (vide infra), we found a coupling constant J of -65 cm^{-1}. This value is quite similar to that found for the octahedral [(tmeda)(3,6-di-*tert*-butylbenzosemiquinonate)$_2$zinc(II)] complex,[24] which is -33.7 cm^{-1} (tmeda = *N*,*N*,*N*′,*N*′-tetramethylethylenediamine). These measurements establish a singlet ground state for **1** with an energetically low-lying triplet excited state.

The X-band EPR spectrum of **1** in diethyl ether at 30 K shown in Figure 4 exhibits typical features of a spin triplet

(24) Lange, C. W.; Conklin, B. J.; Pierpont, C. G. *Inorg. Chem.* **1994**, *33*, 1276.

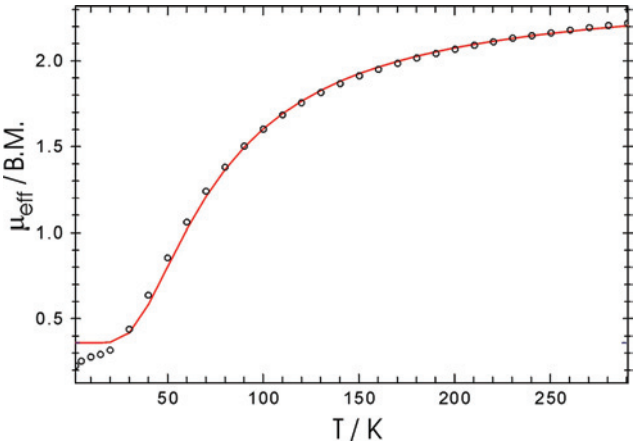

Figure 3. Temperature dependence of the effective magnetic moment of **1**. Open circles represent experimental data points, and the solid line represents a best fit ($H = -2JS_1 \cdot S_2 + \sum_i g_i \mu_B S_i \cdot B$); $S_1 = S_2 = {}^1/_2$; $g_1 = g_2 = 2.006$; $J_{12} = -65$ cm^{-1}). The low-temperature offset is due to a minor paramagnetic impurity (PI) with of 1.6% abundance ($S_{PI} = {}^1/_2$).

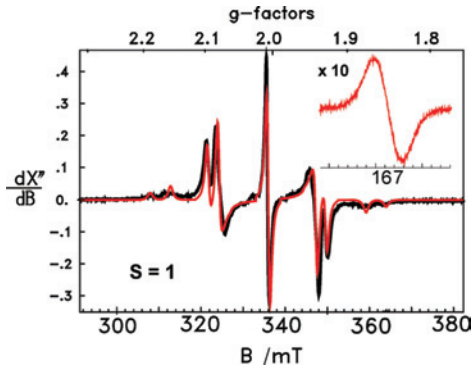

Figure 4. X-band EPR spectrum of a frozen diethyl ether solution of **1** at 30 K and simulation. The inset displays the half-field signal with $\Delta M = 2$. The simulation (red line) is a superposition of three subspectra: two triplet species with isotropic g values, $g = 2.006$, and z components of the axially symmetric dipole coupling matrix $J_z = 0.070$ cm^{-1} (32% relative intensity) and $J_z = 0.058$ cm^{-1} (67%) and an impurity with $S = {}^1/_2$ and $g = 2.0$ (isotropic, 1% intensity). Experimental conditions: frequency 9.433 32 GHz; power 100 μW; modulation 0.5 mT/100 kHz.

with weak zero-field splitting: There are two strong, symmetrically split main transitions with weaker outer satellite lines that are all centered at $g = 2$ and a weak half-field signal at $g = 4$ due to "forbidden" transitions with $\Delta M = 2$. The spectrum apparently arises from the $S_t = 1$ excited state of the diradical complex. Very similar results have been reported for other diradical complexes $[Zn^{II}(L^{\bullet})_2]$ with a tetrahedral ZnN_4 polyhedron ($L^{\bullet}$ = α-diiminate).[8a,25] However, the EPR transitions of **1** show additional splitting each, which indicates the presence of two slightly different species. Accordingly the spectrum could be readily simulated with a superposition of two triplet subspectra with different zero-field splitting, due to different intramolecular dipole interactions between the radicals. In terms of the traceless dipole coupling matrix, the subspectra are characterized by main values $J_z = 0.070$ cm^{-1} (32% intensity) and $J_z = 0.058$ cm^{-1} (67%). At $g = 2.0$, the observed sharp isotropic signal is attributed to an $S = {}^1/_2$ impurity (~1%). We propose that the two triplet subspectra correspond to a five-coordinate

(25) Lu, C. C.; Bill, E.; Weyhermüller, T.; Bothe, E.; Wieghardt, K. *J. Am. Chem. Soc.* **2008**, *130*, 3181.

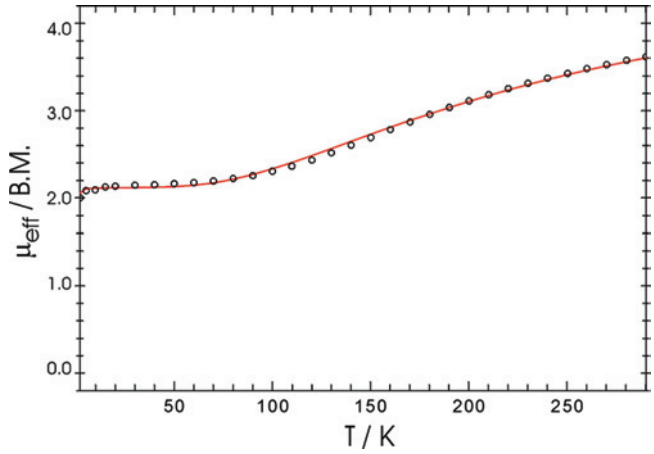

Figure 5. Temperature dependence of the effective magnetic moment of **2**. Open circles are experimental data points, and the solid line is a best fit of the data (see the text for details).

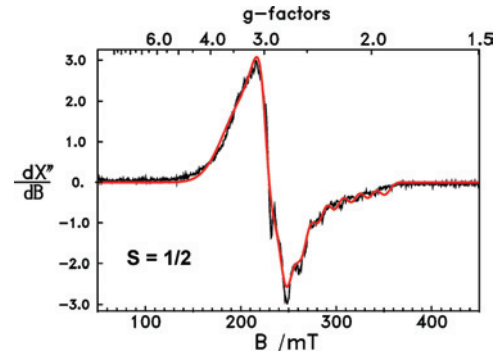

Figure 6. X-band EPR spectrum of a frozen diethyl ether solution of **2** at 30 K. Simulation (red line) parameters are given in the text. Conditions: frequency 9.428 43 GHz; power 100 μW; modulation 1 mT/100 kHz.

$[Zn^{II}(L^{\bullet})_2(Et_2O)]^0$ and a four-coordinate $[Zn^{II}(L^{\bullet})_2]$ species, which are in equilibrium in solution.

Figure 5 displays the temperature dependence of the effective magnetic moment of a solid sample of **2**. The values of μ_{eff} decrease monotonically from 3.6 μ_B at 290 K to a plateau of 2.1 μ_B in the range 70−10 K. This behavior has been modeled for a tetrahedral cobalt(II) center ($S_{Co} = {}^3/_2$) O,O′-coordinated to two ligand radicals ($S_{rad} = {}^1/_2$) by using the spin Hamiltonian equation (1).

$$H_{ex} = -2J(\vec{S}_{rad1} + \vec{S}_{rad2}) \cdot \vec{S}_{Co} + g_{rad}\mu_B(\vec{S}_{rad1} + \vec{S}_{rad2}) \cdot \vec{B} + g_{Co}\mu_B \vec{S}_{Co} \cdot \vec{B} \quad (1)$$

The intramolecular antiferromagnetic coupling between a ligand π radical ($S_{rad} = {}^1/_2$) and a central cobalt(II) ion $S_{Co} = {}^3/_2$ is found to be relatively weak ($J = -80$ cm^{-1}). The excellent fit shown in Figure 5 was obtained without considering ligand-to-ligand coupling between the two π radicals, which is probably weak. The relatively high plateau of μ_{eff} at low temperatures reveals a $S_t = {}^1/_2$ ground state with a large g value due to the local contribution from the cobalt(II) ion with $g_{Co} = 2.43$ (g_{rad} was fixed to 2.0).

The X-band EPR spectrum of **2** in frozen diethyl ether at 30 K shown in Figure 6 displays a rhombic $S = {}^1/_2$ signal with $g_x = 3.45$, $g_y = 2.81$, and $g_z = 2.32$ and with hyperfine coupling constants of $A_{xx} = 17 \times 10^{-4}$ cm^{-1}, $A_{yy} = 34 \times 10^{-4}$ cm^{-1}, and $A_{zz} = 190 \times 10^{-4}$ cm^{-1}. By using spin

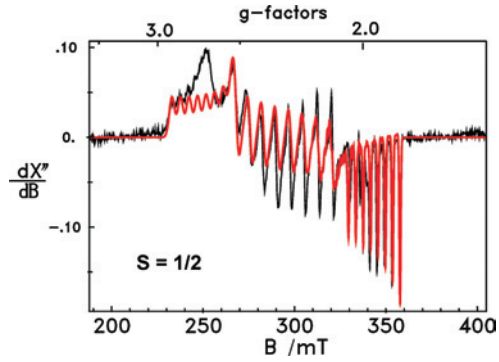

Figure 7. X-band EPR spectrum of a frozen diethyl ether solution of **4** at 30 K. Simulation (red line) parameters are given in the text. Conditions: frequency 9.431 20 GHz; power 10 μW; modulation 0.4 mT/100 kHz.

projection techniques [$g_t = {}^5/_3 g_{Co} - {}^2/_3 g_{rad}$; $g_{Co} = {}^3/_5(g_t + {}^2/_3 g_{rad})$], we arrive at local values $g_{Co} = 2.53$ ($g_x = 2.87$, $g_y = 2.49$, and $g_z = 2.19$) and ^{59}Co hyperfine coupling constants ($A_{Co} = {}^3/_5 A_t$) of 10×10^{-4}, 20×10^{-4}, and 114×10^{-4} cm^{-1}. These data corroborate the proposed $S_t = {}^1/_2$ ground state for **2**.

The effective magnetic moment of **4** was found to be temperature independent at 2.1 μ_B in the range 5−290 K (see Figure S1 in the Supporting Information). An isotropic g value of 2.46 and the effective magnetic moment indicate an $S_{Co} = {}^1/_2$ ground state for **4**. These values are quite typical for low-spin cobalt(II) in a square-planar ligand field.[26]

The X-band EPR spectrum of **4** in a frozen solution at 30 K is shown in Figure 7. A rhombic signal at $g_x = 2.71$, $g_y = 2.30$, and $g_z = 1.97$ (average $g_{Co} = 2.35$) and ^{59}Co hyperfine coupling constants $A_{xx} = 49 \times 10^{-4}$ cm^{-1}, $A_{yy} = 80 \times 10^{-4}$ cm^{-1}, and $A_{zz} = 37 \times 10^{-4}$ cm^{-1} are in excellent agreement with an $S_{Co} = {}^1/_2$ ground state.

3.5. DFT Calculations. DFT calculations for **1** ($S = 0$ and 1 states) and **2** ($S = {}^1/_2$) have been performed at the B3LYP level using spin-unrestricted methods. BS states, with n spin-up electrons and m spin-down electrons are denoted by the label BS(n,m). This approach is important because it permits the n and m electrons to be localized on different areas of the molecule, i.e., metal versus ligand, so they can be coupled magnetically but are not forcibly paired. The robustness of all BS solutions was checked by complementary calculations without BS. These calculations resulted in all present cases in a higher energy state.

By taking the initial coordinates from the solid-state structures of **1** and **2**, the geometry optimizations of the bis(ligand)metal complexes converged successfully for the given S_{tot} and BS state, namely, for **1** the BS(1,1) $S = 0$ and $S = 1$ states and for **2** the BS(3,2) $S = {}^1/_2$ state.

In all of the converged structures, the two ligands are identical and, in general, we observe excellent agreement between the experimental and calculated structures (Table 4). The calculated C−O and C−C bond distances of the chelate rings agree within ±0.005 Å with the experiment. The calculated metal−ligand bond lengths are overestimated by ~0.07 Å, which is quite typical for the B3LYP functional.

Interestingly, the corresponding C−O and carbonyl C−C bonds in all calculations of **1** ($S = 0$, 1) and **2** are identical and indicative of the presence of the π-radical monoanionic oxidation level (Table 4). In contrast in $Na_2(Et_2O)_2[V^{IV}(L^{Red})_3]$, these distances have been calculated (and experimentally verified)[3] to be at 1.35 (C−O) and 1.40 Å (C−C), indicating the presence of closed-shell dianions $(L^{Red})^{2-}$.

The electronic structure of **1** has been calculated using the BS(1,1) method for $S = 0$ and 1 states. Interestingly, the singlet state is calculated to be more stable by only ~32 cm^{-1} than the triplet state; thus, both states are calculated to be nearly isoenergetic. Experimentally, it was shown from magnetic susceptibility measurements that the singlet state is lower in energy than the triplet by 130 cm^{-1}. Figure 8 shows the spin-density plots for both states from a Mulliken population analysis. Clearly, each ligand carries one unpaired electron. The spins are aligned in the triplet state but antiparallel in the singlet. The central zinc(II) ion (d^{10}) does not have any spin density.

Figure 9 displays a qualitative MO diagram for **2**, where the corresponding orbitals[17] of magnetic pairs are shown as derived from a BS(3,2) DFT calculation. Five metal-centered d orbitals are identified, two of which are doubly filled and three of which are singly occupied. This is the hallmark of a cobalt(II) ion (d^7, $S_{Co} = {}^3/_2$). In addition, two ligand-centered singly occupied MOs (SOMOs) are identified, which couple antiferromagnetically with two metal SOMOs, giving rise to the observed $S_t = {}^1/_2$ ground state. The single unpaired electron occupies a metal d orbital in agreement with its EPR spectrum.

Figure 10 exhibits the spin density in **2**. The cobalt(II) ion carries +2.7 α spins (red), and both ligands carry −0.28 β spins (yellow) on each of the carbonyl carbon atoms and −0.19 β spins on each of the oxygen donors. Thus, there are three unpaired electrons at the cobalt center and one unpaired electron on each ligand π-radical anion: $[Co^{II}(L^{\bullet})_2(Et_2O)]^0$ ($S_t = {}^1/_2$).

The corresponding DFT calculations for the monoanion in **3** and the dianion in **4** ($S = {}^1/_2$) have also been performed at the B3LYP level. For $[Co(L)_2]^-$, two solutions with $S =$ 1 and 0 ground states have been calculated. It was found that the triplet state is 9.7 kcal/mol lower in energy than the closed-shell $S = 0$ state. Therefore, we discuss only the triplet state for this monoanion in the following. By taking the initial coordinates from the solid-state structures of **3** and **4**, the geometry optimizations converged successfully for the respective given S states. In both converged structures, the geometrical features of the two ligands are identical and are indicative of the presence of closed-shell enediolate(2−) dianions $(L^{Red})^{2-}$. Agreement between the experimental and calculated structures (Table 4) is excellent. We note that the calculated C−C bond length of the O,O-coordinated diketone is longer than the observed one by 0.047 Å, which is a surprisingly large discrepancy and may be a consequence of the fact that we calculated the dianion without the two sodium cations.

Table 4. Comparison of Experimental and Calculated Bond Distances in **1** and **2**

	1		
		calcd	
	expt	$S = 0$	$S = 1$
Zn(1)−O(1)	1.971(1)	2.035	2.031
Zn(1)−O(2)	2.051(1)	2.047	2.063
Zn(1)−O(31)	1.971(1)	2.041	2.045
Zn(1)−O(32)	2.054(1)	2.062	2.049
Zn(1)−O(63)	2.083(1)	2.183	2.181
O(1)−C(1)	1.290(1)	1.291	1.290
O(2)−C(2)	1.281(1)	1.288	1.281
C(1)−C(2)	1.440(1)	1.455	1.439
O(31)−C(31)	1.288(1)	1.290	1.288
O(32)−C(32)	1.281(1)	1.287	1.281
C(31)−C(32)	1.439(1)	1.454	1.440

	2		**3**		**4**	
	expt	calcd $S = {}^1/_2$	expt $S = 1$	calcd $S = 1$	expt $S = {}^1/_2$	calcd $S = {}^1/_2$
Co(1)−O(1)	1.944(1)	1.984	1.837(2)	1.853	1.8659(8)	1.868
Co(1)−O(2)	2.071(1)	2.133	1.831(2)	1.850	1.8767(9)	1.871
Co(1)−O(31)	1.937(1)	2.027				
Co(1)−O(32)	2.095(1)	2.029				
Co(1)−O(63)	2.064(1)	2.156				
O(1)−C(1)	1.299(1)	1.297	1.345(3)	1.365	1.373(1)	1.354
O(2)−C(2)	1.284(1)	1.280	1.345(3)	1.365	1.374(1)	1.357
C(1)−C(2)	1.445(1)	1.443	1.384(3)	1.387	1.360(2)	1.407
O(31)−C(31)	1.297(1)	1.290				
O(32)−C(32)	1.281(1)	1.287				
C(31)−C(32)	1.443(1)	1.445				

The electronic structure of the dianion in **4** has been calculated for the $S = {}^1/_2$ state. The single unpaired electron occupies a metal d orbital (81%), and three predominantly metal d orbitals are doubly occupied. This is typical for a low-spin cobalt(II) ion (d^7, $S_{Co} = {}^1/_2$). The qualitative bonding scheme as derived from the spin-unrestricted B3LYP DFT calculation is shown in Figure S4 in the Supporting Information. A Mulliken spin-density population analysis (Figure 11) revealed that there is almost no spin density on the ligands, but one unpaired electron resides at the metal ion. Thus, the calculated electronic structure of **4** is best described as $Na_2(Et_2O)_4[Co^{II}(L^{Red})_2]$ ($S = {}^1/_2$).

In contrast, the situation for the monoanion in **3** is more complex. The d-orbital population at the central cobalt ion decreases upon oxidation of **4** (as expected), while the spin-density population increases to more than 1.45 unpaired electrons (Table 5). Both observations apparently indicate that the central cobalt is oxidized to a cobalt(III) ion with $S = 1$ upon one-electron oxidation of the dianion **4**, while the ligands exist in the dianionic form $(L^{Red})^{2-}$. This is also in accordance with the interpretation of the structural data.

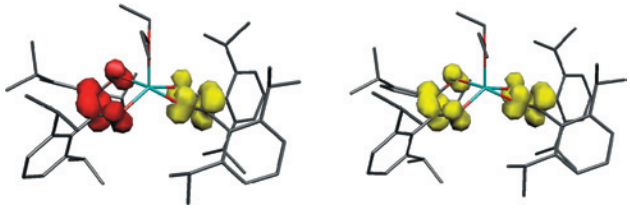

Figure 8. Spin-density plots for (nearly) isoenergetic $S = 0$ (left) and $S = 1$ (right) states of **1** (from a Mulliken spin-density population analysis): α spin in red; β spin in yellow. In both states, there is a spin-density population of ∼1 electron/ligand (±0.54 on the two carbon atoms of each ligand and ±0.42 on the two oxygen atoms).

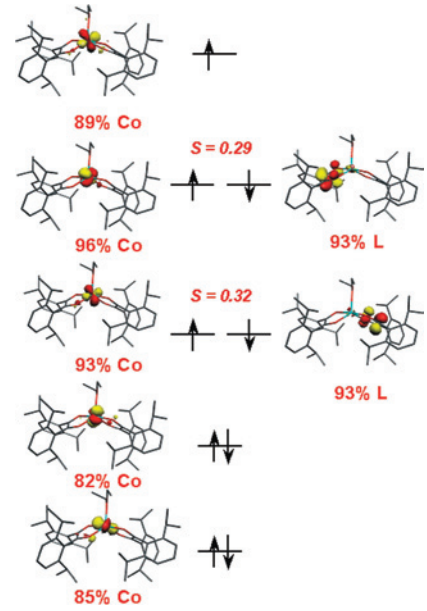

Figure 9. Qualitative MO scheme of the corresponding orbitals of magnetic pairs of **2** as derived from BS(3,2) DFT calculation. Values of the overlap integral S close to 1 indicate a standard doubly occupied MO, whereas an S value of 0 represents orthogonal magnetic orbitals. Intermediate values for S are the signature of nonorthogonal magnetic orbital pairs, which cause antiferromagnetic coupling between the electrons.

However, as shown previously for square-planar $[Co(^1L_N)_2]^{-27}$ and $[Co(L_{S,S})_2]^{-28}$ $[(^1L_N)^{2-}$ represents the dianion 1,2-benzenediamide(2−) and $(L_{S,S})^{2-}$ is 1,2-ben-

(26) Daul, C.; Schläpfer, C. W.; von Zelewsky, A. *Structure and Bonding*; Springer Verlag: Berlin, 1979; Vol. *36*, p 129.
(27) Bill, E.; Bothe, E.; Chaudhuri, P.; Chlopek, K.; Herebian, D.; Kokatam, S.; Ray, K.; Weyhermüller, T.; Neese, F.; Wieghardt, K. *Chem.—Eur. J.* **2005**, *11*, 204.

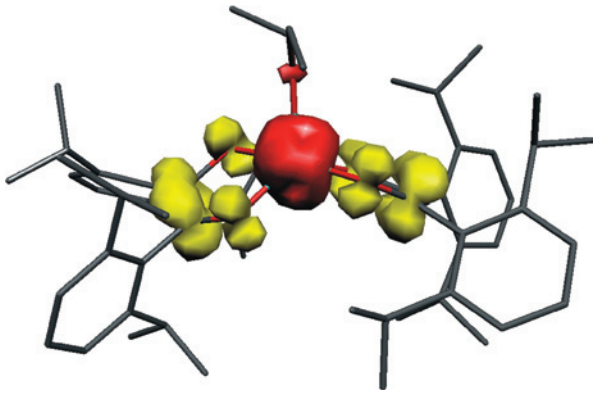

Figure 10. Spin-density plot of **2** from a Mulliken spin-density population analysis for a BS(3,2) DFT calculation (B3LYP). α spin red: +2.7 (~3 electrons). β spin yellow: −0.28 on each carbon and −0.19 on each oxygen (~2.0 electrons).

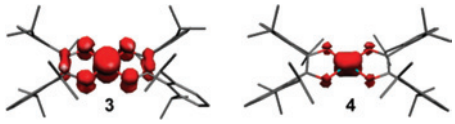

Figure 11. Spin-density plots of **3** (+1.45 on cobalt, +0.09 on each oxygen, and +0.04 on the carbon atoms) and **4** (+0.92 on cobalt and +0.02 on each oxygen) from a Mulliken spin-density population analysis.

Table 5. Comparison of the Charge and Spin-Density Populations at the Cobalt Ions Resulting from a Löwdin Analysis of the One-Electron Density of the Ground State from B3LYP DFT Calculations

	electron d	electron 4s	spin d	spin s
$[Co(L^{Red})_2]^{2-}$ (**4**)	7.72	0.43	0.93	−0.01
$[Co(L^{Red})_2]^{-}$ (**3**)	7.52	0.39	1.45	0.00

zenedithiolate(2−)], both the d population [which is somewhat higher than expected for cobalt(III)] and the spin-density population [Figure 11; which is lower than expected for cobalt(III)] show that the above description is an oversimplification. The actual electronic structure may be better represented by the resonance forms $[Co^{III}(L^{Red})_2]^- \leftrightarrow [Co^{II}(L^{\bullet})(L^{Red})]^- \leftrightarrow [Co^{II}(L^{Red})(L^{\bullet})]^-$ but with a slightly larger weight for the first structure. Note that the DFT calculations clearly show some spin density on the ligand $(L^{Red})^{2-}$, indicating some $(L^{\bullet})^-$ character.

The calculated ground state is $^3B_{1g}$ with the following electronic configuration: $(1a_g)^2(2a_g)^2(1b_{3g})^2(1a_u)^2(1b_{2g})^2(1b_{1u})^2(2b_{2g})^1(2b_{3g})^1(1b_{1g})^0$. The qualitative bonding scheme as derived from the spin-unrestricted B3LYP DFT calculation is shown in Figure S5 in the Supporting Information. The ligand character in the $2b_{2g}$ orbital is found to be quite high (57%).[27,28]

4. Conclusions

The most salient feature of this study is the structural characterization of the mono- and dianionic ligands $(L^{\bullet})^-$ ($S_{Rad} = {}^1/_2$) and $(L^{Red})^{2-}$ in the five-coordinate complexes **1**, **2**, and **4**. Complex **3** is formally the one-electron oxidized form of **4**.

It is shown that **1** possesses an $S = 0$ ground state and an $S = 1$ excited state at 130 cm^{-1} in energy above the ground state. Complex **2** possesses an electronic structure consisting of two π-radical anionic ligands $(L^{\bullet})^-$ and a central high-spin cobalt(II) ion (d^7, $S_{Co} = {}^3/_2$), which are exchange coupled, yielding the observed $S = {}^1/_2$ ground state. In contrast, the four-coordinate, square-planar dianion in **4** consists of two reduced enediolate(2−) ligands and a low-spin cobalt(II) ion (d^7, $S_{Co} = {}^1/_2$). These results have been corroborated by DFT calculations at the B3LYP level.

The electronic structure of the square-planar monoanion $[Co(L)_2]^-$ in **3** is more complicated. DFT calculations suggest an $S = 1$ ground state. Of the three resonance structures $[Co^{III}(L^{Red})_2]^- \leftrightarrow [Co^{II}(L^{\bullet})(L^{Red})]^- \leftrightarrow [Co^{II}(L^{Red})(L^{\bullet})]^-$, it is the first one that has the largest weight, but the other two are also important. It is therefore not possible to assign an unambiguous oxidation state for the central cobalt ion (II or III).

Acknowledgment. We thank the Fonds der Chemischen Industrie for financial support. G.H.S. is grateful to the Alexander von Humboldt Foundation for a stipend.

Supporting Information Available: Experimental and calculated bond lengths (Å) for **1** (Table S1) and for **2** (Table S2), temperature dependence of the magnetic moment of solid **4** (Figure S3), and qualitative bonding schemes for the dianion in **4** and the monoanion in **3** (Figures S4 and S5, respectively). This material is available free of charge via the Internet at http://pubs.acs.org.

IC801470P

(28) Ray, K.; Begum, A.; Weyhermüller, T.; Piligkos, S.; van Slageren, J.; Neese, F.; Wieghardt, K. *J. Am. Chem. Soc.* **2005**, *127*, 4403.